JACS
JOURNAL OF THE AMERICAN CHEMICAL SOCIETY
pubs.acs.org/JACS
Article

A Bioinspired Disulfide/Dithiol Redox Switch in a Rhenium Complex as Proton, H Atom, and Hydride Transfer Reagent

Shao-An Hua, Lucas A. Paul, Manuel Oelschlegel, Sebastian Dechert, Franc Meyer,* and Inke Siewert*

Cite This: J. Am. Chem. Soc. 2021, 143, 6238–6247
Read Online

ABSTRACT: The transfer of multiple electrons and protons is of crucial importance in many reactions relevant in biology and chemistry. Natural redox-active cofactors are capable of storing and releasing electrons and protons under relatively mild conditions and thus serve as blueprints for synthetic proton-coupled electron transfer (PCET) reagents. Inspired by the prominence of the $2e^-/2H^+$ disulfide/dithiol couple in biology, we investigate herein the diverse PCET reactivity of a Re complex equipped with a bipyridine ligand featuring a unique SH···$^-$S moiety in the backbone. The disulfide bond in *fac*-[Re($^{S-S}$bpy)(CO)$_3$Cl] (**1**, $^{S-S}$bpy = [1,2]-dithiino[4,3-*b*:5,6-*b*′]dipyridine) undergoes two successive reductions at equal potentials of −1.16 V vs $Fc^{+|0}$ at room temperature forming [Re(^{S2}bpy)(CO)$_3$Cl]$^{2-}$ (**1**$^{2-}$, ^{S2}bpy = [2,2′-bipyridine]-3,3′-bis(thiolate)). **1**$^{2-}$ has two adjacent thiolate functions at the bpy periphery, which can be protonated forming the S−H···$^-$S unit, **1**H$^-$. The disulfide/dithiol switch exhibits a rich PCET reactivity and can release a proton ($\Delta G°_{H^+}$ = 34 kcal mol^{-1}, pK_a = 24.7), an H atom ($\Delta G°_{H^\bullet}$ = 59 kcal mol^{-1}), or a hydride ion ($\Delta G°_{H^-}$ = 60 kcal mol^{-1}) as demonstrated in the reactivity with various organic test substrates.

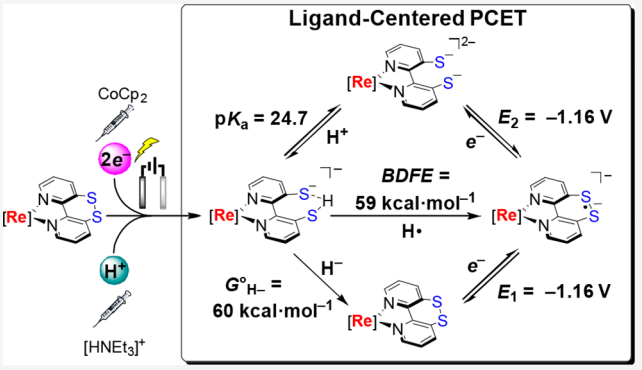

INTRODUCTION

The synchronized transfer of electrons and protons is a critical step in many chemical and biological transformations. In particular, hydride and H atom transfer reactions are important in, for example, catalytic hydrogenation, hydroformylation, or small molecule activation reactions relevant to renewable energy storage. This has stimulated extensive research on hydride and H atom donor reagents, metal and nonmetal containing, as reducing agents during the past decades.[1−14] Inspired by natural enzymatic cofactors, for example, nicotinamide adenine dinucleotide phosphate (NADPH) or flavin adenine dinucleotide ($FADH_2$), several nonmetal hydride donors with dihydropyridines or dihydroquinoline moieties have been established.[15] $FADH_2$ acts as a hydride donor in various biochemical processes. For example, it is used as redox reagent by glutathione reductase and thioredoxin reductase, which mediate the glutathione disulfide to glutathione conversion[16−18] or thioredoxin reduction,[19] respectively. Synthetic analogues of such hydride donors, for example, Hantzsch esters, have been widely explored in (asymmetric) hydrogenation reactions.[20−27]

The formation (or regeneration) of nonmetal hydride donors from the conjugated species is usually challenging. The use of strong hydrogenation reagents such as H_2 over Pd/C or $LiAlH_4$ can lead to over- or nonselective reduction. Electrochemical regeneration by consecutive single electron transfer steps and protonation often produces highly reactive radical species as intermediates, which have a strong tendency to, for example, dimerize instead of undergoing the desired $1H^+/1e^-$ follow-up reactivity. To modulate the redox properties and reactivity of the singly reduced intermediates, such hydride donors have been combined with redox-active metal ions.[28] Pioneering work of Tanaka and co-workers showed that a ruthenium complex equipped with a NAD-type model ligand can be used for facile and selective hydride transfer to, for example, CO_2.[29−32] The electrochemical regeneration via $2e^-/H^+$ transfer can be achieved at moderate potentials. Similarly, the stoichiometric hydrogen transfer reactivity of a proton responsive azo unit in the coordination sphere of Co(I) ions has recently been explored.[33] The complex is accessible via electrochemical $2e^-/H^+$ reduction at a moderate potential and exhibits a versatile PCET reactivity, viz. $2e^-/H^+$ and e^-/H^+ transfer. Another example of ligand-centered NH group PCET reactivity has recently been reported for Ni(II), Pd(II), and Pt(II) pincer complexes with a coordinated amide/amine functionality.[34,35] The solution bond dissociation free energy

Received: February 14, 2021
Published: April 16, 2021

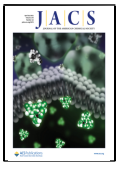

https://doi.org/10.1021/jacs.1c01763
J. Am. Chem. Soc. 2021, 143, 6238−6247

(BDFE) of the N−H unit was found to increase by about 10 kcal mol^{-1} within the group as the pK_a and the redox potential increase.

Inspired by the natural disulfide/dithiol 2H$^+$/2e$^-$ couple,[36−38] we introduced recently a 2,2′-bipyridine that is equipped with a disulfide/dithiolate unit in the backbone for storing multiple electrons.[39] The 2e$^-$ redox interconversion is associated with a smooth rotation around the central bipyridine C−C bond to minimize Coulombic and steric repulsion in the dithiolate form, which adopts an angle of ∼90° between the two pyridine rings (Scheme 1, $^{S-S}$bpy = 1,2-

Scheme 1. Two-Electron Redox Interconversion of the Disulfide/Dithiolate Couple in the $^{S-S}$bpy Ligand[37] and a Ru Photosensitizer[40,41]

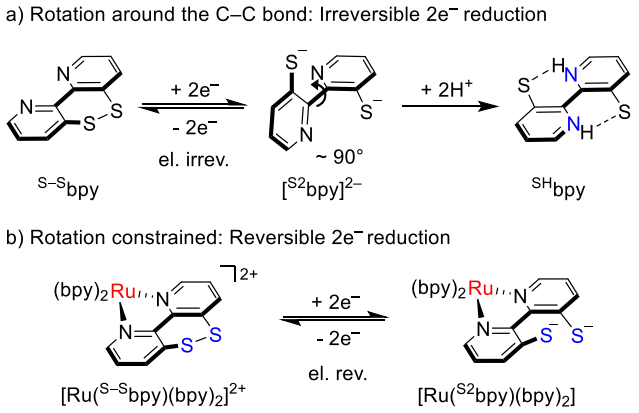

dithiino[4,3-*b*:5,6-*b*′]dipyridine).[39] However, these large structural changes lead to slow, irreversible electron transfer rates for the redox processes. Subsequent protonation of the reduced ligand (^{S2}bpy)$^{2-}$ appears at the nitrogen donor sites as these are more basic, and this induces a rotation by an additional 90° due to a hydrogen bond between the NH and −S$^-$ units. To facilitate the electron transfer, $^{S-S}$bpy was attached to a metal template as this constrains rotation around the central C−C bond. Indeed, when bound to a Ru^{II} ion via the *N*,*N*′-chelate as in [Ru($^{S-S}$bpy)(bpy)$_2$]$^{2+}$ (Scheme 1), the two reduction processes induce rather small structural reorganizations and thus appear almost reversible.[40] Additionally, a potential inversion for the first and second reduction step occurs. Notably, the destabilization of [Ru(^{S2}bpy)(bpy)$_2$] due to the rather short S$^-$···S$^-$ distance in the dithiolate form compared to the free ligand is compensated by the polarization effect due to metal ion binding as the oxidations of [Ru(^{S2}bpy)(bpy)$_2$] and (^{S2}bpy)$^{2-}$ appear at similar potentials.[39,40]

A metal template thus provides the ideal platform to couple the readily accomplishable 2e$^-$ disulfide/dithiolate interconversion of $^{S-S}$bpy with a proton transfer as it also blocks the more basic N site. Herein, we exploit now such a unique S−S/SH···$^-$S unit in the coordination sphere of a redox-silent Re(CO)$_3$ moiety, and we report on its facile 2e$^-$, 2e$^-$/1H$^+$ (viz. hydride), e$^-$/H$^+$ (viz. H$^•$), and H$^+$ interconversion as outlined in Scheme 2. Previous work on proton triggered redox isomerization of disulfide/thiol units involved redox-active copper(II/I) ions,[42,43] whereas in the present system, the electrons and protons are stored exclusively in the ligand. *fac*-[Re($^{S-S}$bpy)(CO)$_3$Cl] (**1**) has been synthesized previously and immobilized on gold electrodes via the peripheral

Scheme 2. Ligand-Centered PCET Reactivity of the $^{S-S}$bpy Ligand Attached to the Re(CO)$_3$ Template, Which Is the Subject of This Study

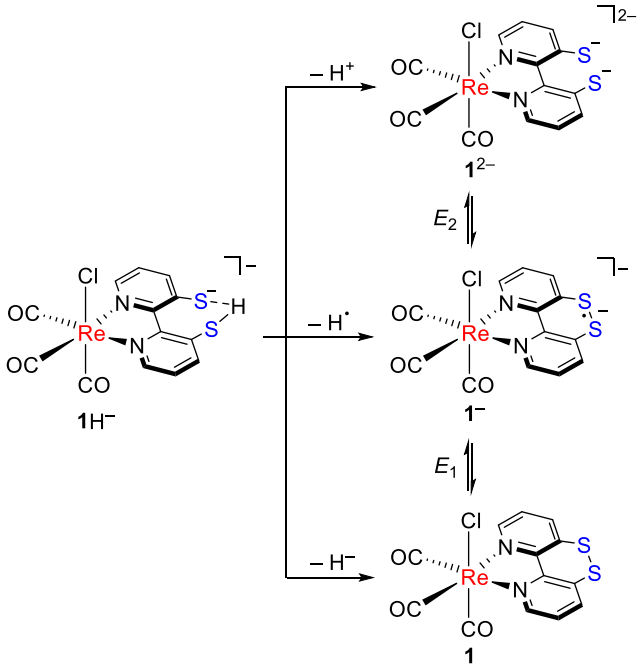

dithiolate anchor with the aim of investigating it as a heterogenized CO$_2$ electroreduction catalyst.[44] Here we report the comprehensive characterization of **1**, and we focus on the thermochemistry of the disulfide/dithiol couple and its versatile PCET reactivity (Scheme 2). For the sake of completeness, we also investigated the homogeneous electrochemical CO$_2$ reduction catalysis briefly; these results can be found in section 2 of the Supporting Information.

RESULTS AND DISCUSSION

Synthesis and Characterization. The synthesis of **1** was recently reported via the reaction of the ligand $^{S-S}$bpy with Re(CO)$_5$Cl at moderate temperature (40 °C) to avoid ligand decomposition, viz. the formation of the related complex *fac*-[Re(^{S}bpy)(CO)$_3$Cl], **2**, with the monosulfur ^{S}bpy ligand (^{S}bpy = thieno[3,2-*b*:4,5-*b*′]dipyridine). This approach, however, resulted in a moderate synthetic yield (∼21%) and limited purity of the desired complex.[44] In this work, we now follow the typical procedure for the synthesis of *fac*-[Re(bpy)(CO)$_3$Cl]-type complexes by heating a toluene solution of $^{S-S}$bpy and Re(CO)$_5$Cl at 100 °C for 1 h.[45] After work-up, analytically pure **1** was isolated in 90% yield as confirmed by combustion analysis. Notably, no decomposition of **1** yielding **2** was observed via this route. Direct synthesis of **2** can be achieved with a synthetic yield of 75% by following the same protocol employing thieno[3,2-*b*:4,5-*b*′]dipyridine as a ligand. The spectroscopic characterization, including NMR, IR, and UV−vis spectra, and ESI-MS of **1** and **2** are given in the Supporting Information. Single crystals of **1** were obtained by vapor diffusion of diethyl ether into a solution of **1** in CH$_2$Cl$_2$. The unit cell of **1** contains two crystallographically independent molecules with similar bond lengths and angles, and the structure of one of them is depicted in Figure 1 together with selected structural parameters (metric parameters of the second molecule are given in Table S5). All details

https://doi.org/10.1021/jacs.1c01763
J. Am. Chem. Soc. 2021, 143, 6238−6247

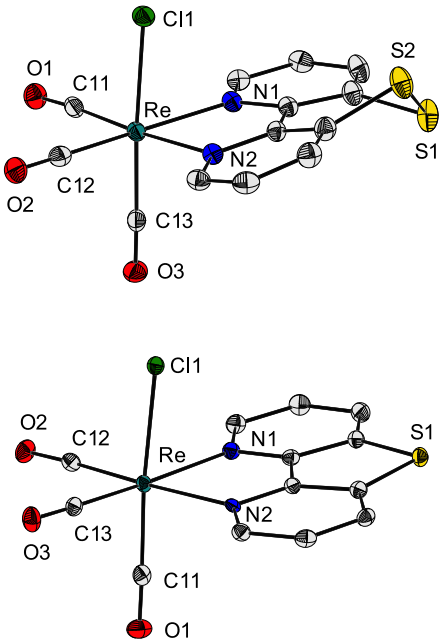

Figure 1. One of the two crystallographically independent molecules of **1** (top) and molecular structure of **2** (bottom) shown as 50% probability thermal ellipsoids. Hydrogen atoms omitted for clarity. Selected structural parameters of distances (Å) and torsion angles (deg) for **1**: Re−N1, 2.175(4); Re−N2, 2.166(4); Re−Cl1, 2.474(1); Re−C11, 1.918(6); Re−C12, 1.924(6); Re−C13, 1.921(6); S1−S2, 2.042(2); C−S1−S2−C, 55.9; N1−C−C−N2, 8.6; for **2**: Re−N1, 2.211(2); Re−N2, 2.215(2); Re−Cl1, 2.4879(7); Re−C11, 2.4879(7); Re−C12, 1.908(3); Re−C13, 1.918(3); N1−C−C−N2, 1.1.

related to the X-ray data refinement are summarized in section 3 of the Supporting Information. In agreement with IR spectroscopy, the three carbonyl ligands occupy one face of the octahedron. The Re−N1 and Re−N2 distances are very similar to values reported for comparable rhenium complexes with α-diimine ligands.[46] The disulfide bridge at the backside of the bipyridine leads to a highly distorted six-membered ring with S−S distance of 2.042(2) Å and C−S−S−C torsion angle of 55.9°. These parameters are similar to those found in $[Ru(^{S-S}bpy)(bpy)_2](PF_6)_2$[40] but far away from the ideal C−S−S−C torsion angle of 90° for disulfide moieties.[47] The disulfide clamp at the bipyridine backside leads to a slight tilting of the two pyridine units, as shown by the N1−C−C−N2 torsion angle of 8.6°. Single crystals suitable for X-ray diffraction experiments were also obtained for **2**, and the results confirmed the proposed structure. The two pyridine rings are almost coplanar and bridged by a single sulfur atom forming a five-membered ring (Figure 1). The metric parameters of **2** are given in Table S5.

Cattaneo et al. reported on the slow conversion of **1** forming **2**,[44] and we observed slow decomposition of the doubly reduced, dithiolate species $[Ru(^{S2}bpy)(bpy)_2]$ at room temperature (rt) to give the ^{S}bpy-ligated complex.[40] Thus, we assessed at first the stability of **1**, its doubly reduced species $\mathbf{1}^{2-}$, and the reduced and protonated species $\mathbf{1}H^-$ in solution (Scheme 2). **1** is stable at rt for more than 10 days as monitored by ^{1}H NMR spectroscopy (Figure S17). $\mathbf{1}^{2-}$ was prepared *in situ* by adding 2.0 equiv of cobaltocene ($CoCp_2$) to **1** at −30 °C in MeCN-d_3. The ^{1}H NMR spectrum showed three high field shifted ^{1}H resonances with regard to **1**, consistent with the formation of a C_s-symmetric, electron-rich dithiolate functionality on the backside of the bipyridine ligand that retains the bidentate N,N coordination mode (Figure S16). There is no evidence for structural isomerization, that is, for any switch to a N,S$^-$ coordination mode as observed upon photoexcitation of $[Re(bpy(O^-)_2)(CO)_3Cl]^{2-}$ bearing two RO$^-$ functionalities, viz. the [2,2′-bipyridine]-3,3′-bis(olate) ligand.[48,49] $\mathbf{1}^{2-}$ is not stable toward formation of **2** at rt. Within 5 min, 35% conversion was observed by ^{1}H NMR spectroscopy and after 3 h about 85% (Figure S18). However, the conversion can be suppressed either by lowering the temperature or by protonation of the peripheral dithiolate group. The ^{1}H NMR spectrum of $\mathbf{1}^{2-}$ recorded at −30 °C revealed no formation of **2** after 24 h (Figure S19). Protonation of $\mathbf{1}^{2-}$ with $[HNEt_3]PF_6$ results in the formation of $\mathbf{1}H^-$, which showed only 10% conversion to **2** after 8 h at 25 °C. At −30 °C, it is stable for more than 24 h (Figures S20 and S21; for the choice of $CoCp_2$/$[HNEt_3]PF_6$ for reduction/protonation, see below). The ^{1}H NMR spectrum of $\mathbf{1}H^-$ showed that the complex retains mirror symmetry and that the ligand scaffold holds the same coordination mode as in $\mathbf{1}^{2-}$. The ^{1}H signals are downfield shifted with regard to $\mathbf{1}^{2-}$ since the negative charges on the thiolate groups are compensated by protonation (Figure S16). A broad peak at 13 ppm can be attributed to the S−H···$^-$S hydrogen-bonded proton.

Redox Chemistry of 1. The redox properties of **1** were explored by means of electrochemical, chemical, and spectroscopic methods. All cyclic voltammetry (CV) data were recorded in acetonitrile with $[^nBu_4N]PF_6$ as electrolyte, glassy carbon disk as working electrode, and referenced internally vs $Fc^{+|0}$. CV measurements of **1** at rt reveal an initial reduction process with a peak potential $E_{pc,1} = -1.22$ V and a reverse feature at $E_{pa,1} = -1.11$ V as well as a second irreversible process at −2.56 V ($\nu = 0.1$ V s^{-1}, Figure S5a). The initial reduction of **1** occurs at a significantly less negative potential than in $[Re(bpy)(CO)_3Cl]$[50] and at a similar potential as the 2e$^-$ disulfide reduction in $[Ru(^{S-S}bpy)(bpy)_2]^{2+}$ (cf. $E_1 = -1.16$ V).[40] Thus, we assume that this process is associated with the formation of the dithiolate ligand, and the large current in the forward scan supports a 2e$^-$ reduction event. The peak potential of the first reduction shifts with increasing scan rate and the reoxidation process gets broader and also shifts, indicating a slight degree of (electro)chemical irreversibility (Figure S5a). Yet, the reversibility even at slow scan rates indicates that reductive disulfide cleavage is not associated with chloride ion loss and that $[Re(^{S2}bpy)(CO)_3Cl]^{2-}$, $\mathbf{1}^{2-}$, is stable on the time scale of the CV experiment. Further reduction of $\mathbf{1}^{2-}$ appears at a rather negative potential, which is a shift of about −0.74 V compared to the initial reduction of $[Re(bpy)(CO)_3Cl]$,[50] probably due to the negative charge in $\mathbf{1}^{2-}$. The process is irreversible and shifts cathodically with increasing scan rate, likely due to the rapid dissociation of chloride as follow-up chemical reaction. Controlled-potential coulometry at both rt and −35 °C in MeCN with 0.2 M trifluoroethanol (TFE) confirmed that initial reduction is a 2e$^-$ process and that the complex degrades slowly at rt forming **2** but is stable at −35 °C (Figure S6). Coulometry at −1.40 V for 2 h led to the injection of two charge equivalents at rt, and the thus-formed species was identified electrochemically as **2** by examining an authentic sample of **2** by CV (full CV examination of **2** is given in Figures S5b and S7−S9). When the temperature was decreased to −35 °C, only minor formation of **2** was observed after 2 h

https://doi.org/10.1021/jacs.1c01763
J. Am. Chem. Soc. 2021, 143, 6238−6247

electrolysis according to the subsequent CV experiment (Figure S6d).

Because $\mathbf{1}^{2-}$ proved to be more stable at low temperature, additional CV data at −35 °C were collected (Figure S5a). Initial reduction of **1** at $E_{pc,1}$ = −1.29 V is a two-electron process with a reoxidation wave at −0.98 V. The reoxidation wave is broader than at rt and anodically shifted, which indicates a slower electron transfer rate with decreasing temperature. In line with this, the oxidation and reduction wave shift with increasing scan rate is characteristic for an electrochemically quasi-reversible or irreversible process. The second reduction process is again irreversible and appears at −2.56 V, which is at the same potential as at rt (ν = 0.1 V s^{-1}).

The electrochemical reduction of **1** forming $\mathbf{1}^{2-}$ is chemically reversible at low temperature as investigated by UV−vis spectroelectrochemistry (UV−vis SEC, Figure 2). The

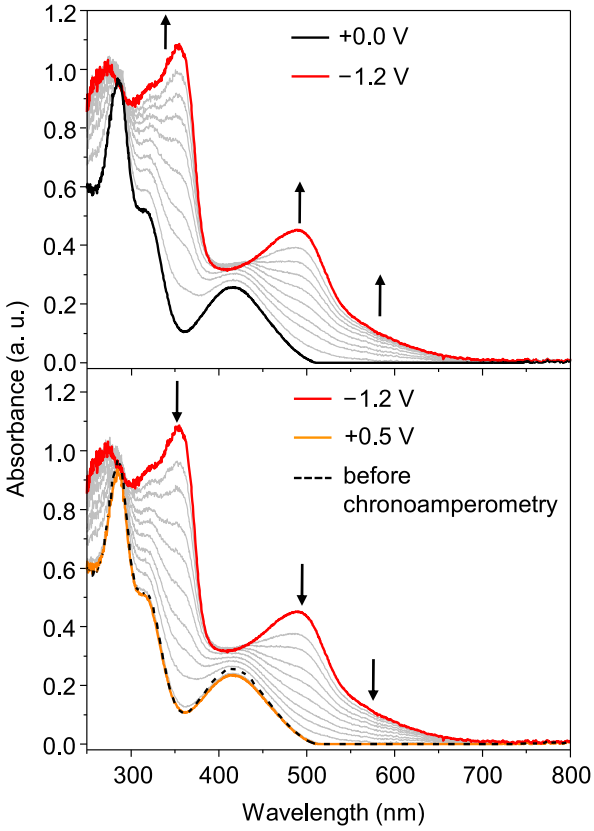

Figure 2. UV−vis SEC spectra during reduction (top) and reoxidation (bottom) of **1** at −35 °C in MeCN, 0.2 M [^{n}Bu$_4$N]PF$_6$.

UV−vis spectrum of **1** in MeCN features the characteristic ligand π−π^* absorption at 285 nm as well as a shoulder at ca. 310 nm and a broad band at 415 nm (Figure S12). According to DFT/TD-DFT computations (B3LYP, 6-31G), the latter two mainly originate from metal-to-ligand charge transfer (MLCT), although IL (intraligand) transitions contribute as well.[51] Two MLCT transitions are calculated at 3.80 eV (S9, 326 nm) and 2.53 eV (S3, 490 nm). The former is primarily an excitation from the Re(dπ) to the bpy(π^*) orbitals, while the latter represents a transition from a Re orbital to a $^{S-S}$bpy ligand orbital that comprises both pyridine units and the disulfide bond (Figure S53 and Table S10). The absorptions of **1** are bathochromically shifted with regard to [Re(bpy)-(CO)$_3$Cl] (cf. λ_{max} = 388, 294, and 240 nm),[52] which reflects the electron-withdrawing effect of the appended disulfide linkage on the π^* orbitals of the bpy ligand.[51]

Electrochemical reduction of **1** at −35 °C at the potential that matches the potential of the first reduction wave led to the clean formation of the new species $\mathbf{1}^{2-}$ with bands at 350 and 490 nm. The steady increase of the intensities of these bands upon reduction is reminiscent of the spectral changes when deprotonating the OH groups on the bpy ligand of [Re(6DHBP)(CO)$_3$Cl] (6DHBP = 6,6′-dihydroxy-2,2′-bipyridine).[53] TD-DFT of the geometry optimized structure of $\mathbf{1}^{2-}$ revealed that the new absorptions centered at ca. 500 nm originate mainly from intraligand charge transfer (ILCT). Two thiolate groups contribute predominantly to the calculated HOMOs, and the LUMOs are made of π-type orbitals on the bipyridine unit (Figure S54 and Table S11). Such an ILCT assignment has been reported also for the related complex [Re(bpy(O$^-$)$_2$)(CO)$_3$Cl]$^{2-}$.[54] The calculated lowest MLCT state (S14) is blue-shifted to ca. 350 nm in comparison to that of **1**, as the LUMO is destabilized because of the accumulation of negative charge and the increased tilting of the two pyridine rings. Electrochemical reoxidation of $\mathbf{1}^{2-}$ at −35 °C led to the formation of **1** with more than 95% spectroscopic yield. The reversible, rather clean reduction and reoxidation of **1** and $\mathbf{1}^{2-}$ support the assumption that $\mathbf{1}^{2-}$ does not eject the chlorido ligand but instead forms a dianionic 18-valence-electron complex.

Finally, **1** was chemically reduced *in situ* with CoCp$_2$ at −30 °C giving $\mathbf{1}^{2-}$ (Scheme 3). CoCp$_2$ has a reduction potential of −1.33 V in CH$_2$Cl$_2$, which is in-between the potential of the first and second reduction processes of **1**.[55] Titration of CoCp$_2$ to a solution of **1** in MeCN at −30 °C results in the clean formation of $\mathbf{1}^{2-}$ as monitored by UV−vis spectroscopy. The absorption at 490 nm reaches its maximum upon adding about 2 equiv of CoCp$_2$, confirming that **1** undergoes a two-electron reduction (Figure S13).

Acid/Base Chemistry of $\mathbf{1}^{2-}$. Because the 2e$^-$ reduction of **1** furnished two peripheral thiolate groups in close proximity, subsequent protonation was investigated. Upon titrating [HNEt$_3$]PF$_6$ to a solution of $\mathbf{1}^{2-}$ in MeCN at −30 °C, the intensity of the absorption bands at 350 and 490 nm steadily decreases up to the addition of about 1 equiv and then remains constant (Figure S14, pK_a(MeCN) = 18.83).[56] This result suggests the formation of singly protonated [Re(^{SHS} bpy)(CO)$_3$Cl]$^-$, $\mathbf{1H}^-$, which has an absorption band at 430 nm and a shoulder at 330 nm. The TD-DFT calculated lowest energy MLCT state at 380 nm (S6) is red-shifted with regard to $\mathbf{1}^{2-}$, indicating that the LUMO on the ligand is stabilized upon protonation (Figure S55 and Table S12). Protonation of the dithiolate moiety is fully reversible, and $\mathbf{1}^{2-}$ was recovered by deprotonation of $\mathbf{1H}^-$ with the strong base ^{t}Bu-P$_1$-(pyrr)$_3$ (pK_a = 28.4 in MeCN, pyrr = pyrrolidino, Figure S15).[57]

To determine the pK_a of $\mathbf{1H}^-$, $\mathbf{1}^{2-}$ was titrated with acetic acid (AcOH) at −30 °C, and the experiment was monitored by UV−vis spectroscopy. Gradual addition of acid leads to the protonation of $\mathbf{1}^{2-}$ forming $\mathbf{1H}^-$ in an equilibrium reaction, as shown in Figure 3. The equilibrium constant between $\mathbf{1}^{2-}$ and AcOH was determined at five representative wavelengths, and the average value for K_{eq} is 15.1 with a standard deviation of 1.5. Acetic acid has a pK_a of 23.51[58] at rt, which leads to a pK_a of 24.7 for $\mathbf{1H}^-$. Notably, we accounted for homoconjugation of acetic acid in solution (see section 4 of the Supporting Information for details). Although the pK_a of $\mathbf{1}^{2-}$ was

https://doi.org/10.1021/jacs.1c01763
J. Am. Chem. Soc. 2021, 143, 6238−6247

Scheme 3. Reactivity and Thermochemical Data of $1/1^{-}/1^{2-}/1H^{-}$ [a]

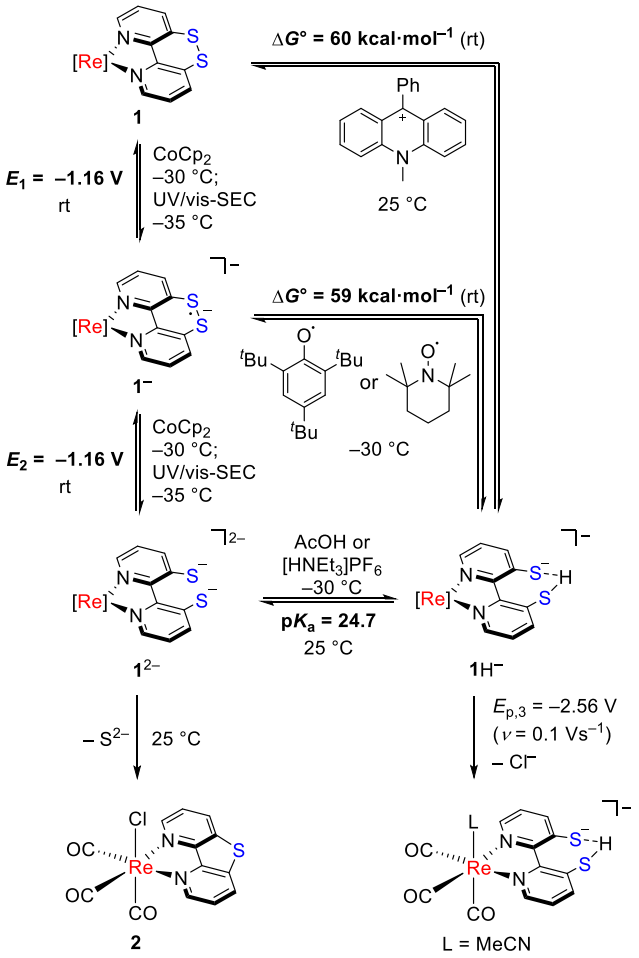

[a]All reactions have been carried out in MeCN; [Re] = {Re(CO)$_3$Cl}.

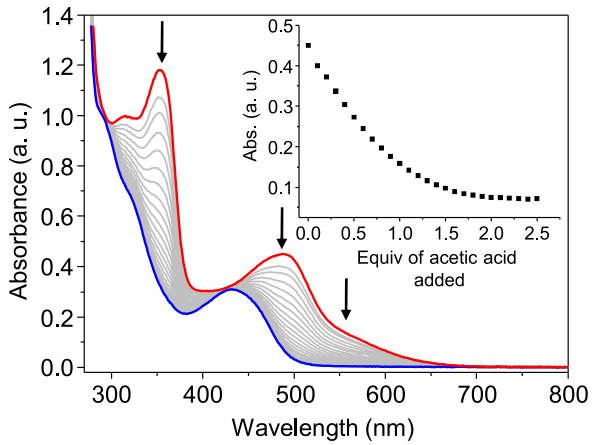

Figure 3. UV–vis spectra of the titration experiment of 1^{2-} with acetic acid at −30 °C in MeCN (start: red trace; end: blue trace; 0.1 equiv steps). Inset: absorbances at 490 nm.

determined at −30 °C, the value serves as a good estimation for the pK_a at rt. The pK_a is temperature-dependent as $-(\partial G/\partial T)_p$ equals ΔS. However, the pK_a at rt for acetic acid was used as reference value, and thus, the value reflects best the pK_a of 1^{2-} at rt (see section 4 of the Supporting Information for details).

Determination of the Hydricity and the S–H BDFE of $1H^{-}$. Following the examinations of the redox processes and protonation on the disulfide/dithiolate couple, the S–H BDFE[59,60] and the hydricity of $1H^{-}$ can be derived via the potential–pK_a method.[61] To establish the thermodynamic cycle, the reduction potentials E_1 and E_2 of **1** were determined with the help of digital simulation of its CV data. The reduction processes at rt and at −35 °C were simulated applying a Butler–Volmer model utilizing CV data over a large scan rate range from 0.1 to 10 V s^{-1}. Representative experimental data and fits are presented in Figure 4. Further

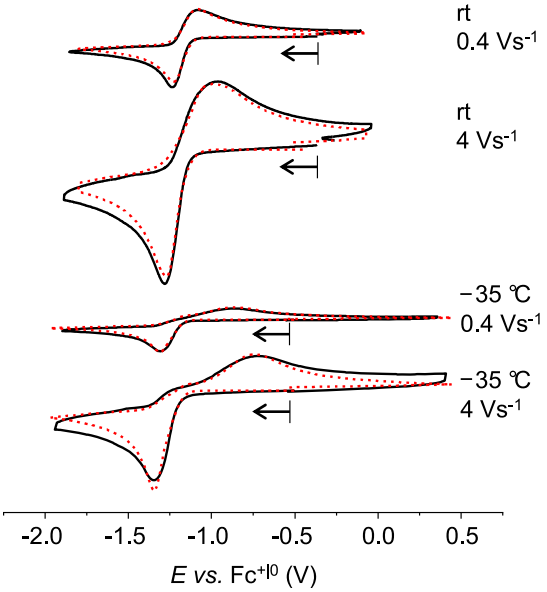

Figure 4. Experimental (black lines) and simulated (red dashed line) CV data of **1** in MeCN, 0.1 M [^{n}Bu$_4$N]PF$_6$; parameters: see Table 1.

figures showing other scan rates at rt and −35 °C are given in the Figures S10 and S11. The slightly broadened reoxidation feature and rather narrow reduction feature indicate an α above 0.5 for at least one of the two 1e$^-$ reductions. The current increase upon reduction was less steep than previously observed in [Ru($^{S-S}$bpy)(bpy)$_2$]$^{2+}$,[40] and indeed, simulation of the data at rt revealed the same potential of −1.16 V for the initial and second reduction at rt. At low temperature, the potential of the initial reduction is slightly more negative than of the following reduction. Good simulations were achieved over a large scan rate range by applying the parameter values shown in Table 1.

As observed in [Ru($^{S-S}$bpy)(bpy)$_2$]$^{2+}$, the geometric constraints impact the reorganization energies of the redox processes.[40] The reorganization energies are smaller in **1** than

Table 1. Thermodynamic and Kinetic Parameters Obtained from the Simulations of the CV Data of 1 at 238 and 298 K

	238 K	298 K
E_1/V	−1.235	−1.16
E_2/V	−1.185	−1.16
α_1	0.4	0.4
α_2	0.8	0.8
k_{s1}/cm s^{-1}	0.005	0.01
k_{s2}/cm s^{-1}	3 × 10^{-4}	0.006

https://doi.org/10.1021/jacs.1c01763
J. Am. Chem. Soc. 2021, 143, 6238–6247

in the free ligand[39] as reflected in the larger electron transfer rates for **1**.

By knowing the pK_a and redox potentials, the hydride donor strength of **1**H$^-$ can be calculated according to eq 1 ($\Delta G^\circ_{(H^+|H^-)}$ = 79.6 kcal mol^{-1}).[8,62]

$$\Delta G^\circ = 1.364\mathrm{p}K_a + 23.06E^\circ_1 + 23.06E^\circ_2 + \Delta G^\circ_{(H^+|H^-)} \quad (1)$$

The free energy for the hydride transfer sums up to 60 kcal mol^{-1} for **1**H$^-$. This is larger than the free energy for the isodesmic reaction of PhS$^-$ and PhSH forming Ph_2S_2 and H$^-$ in dmso, which sums up to only 14 kcal mol^{-1} (Scheme 4, see also section 4 of the Supporting Information for details). This rather high hydricity of PhS$^-$/PhSH can be rationalized by the stabilization of the primary product, the PhS$^\bullet$ radical, by dimerization, which lowers the free energy by about −55 kcal mol^{-1}.[63]

Scheme 4. Individual Free Energy Contributions (kcal mol^{-1}) in the Hydride Transfer Reaction of the Isodesmic Reaction of PhS$^-$ and PhSH in dmso (BDE = Bond Dissociation Energy)

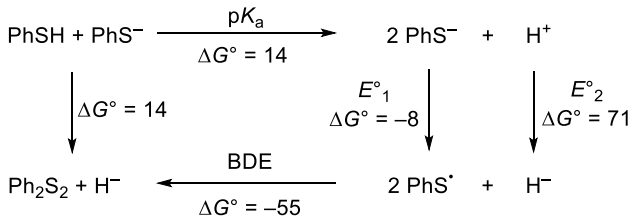

The values for the hydricity of **1**H$^-$ and PhS$^-$/PhSH cannot be compared directly, as one is determined in MeCN and the other one in dmso. Heterolytic S−H bond cleavage leads to charged species, which are stabilized differently depending on the polarity of the solvent.[64−68] However, indirect comparison can be made from the individual free energy contributions (Scheme 4 and Table 2). The difference in the solution free energy of the hydride ion in dmso and MeCN is about 4.8 kcal mol^{-1}.[64] An additional minor contribution in the difference of the hydricity comes from the difference in the pK_a, which is slightly larger in **1**H$^-$ than in PhSH. The latter has a pK_a of 10.3 in dmso, which equals a pK_a of about 21.8 in MeCN considering the difference of the solvation of the proton in MeCN and dmso ($\Delta G_{sol,H^+}$ = 15.7 kcal mol^{-1}, which equals 11.5 pK_a units).[69−71] The nitrogen atom in the ring has likely almost no influence on the BDFE, as estimated from the pK_a differences in 3-pyridinethiol vs thiophenol.[72] The higher pK_a of **1**H$^-$ can be rationalized by its negative charge and the hydrogen bond between the S−H and the adjacent S$^-$ unit, which overbalances the opposite effect arising from metal ion binding of the pyridine units. However, the main contribution for the lower hydricity of **1**H$^-$ arises from differences in the S−S bond strength, that is, the stabilization of the radical R−S$^\bullet$ via dimerization. In **1**$^{2-}$ the contribution of S−S bond formation is included in the oxidation potentials of **1**$^{2-}$ and **1**$^-$ as we have a gradual S···S bond shortening upon oxidation. A free energy gain of −55 kcal mol^{-1} as for PhS$^\bullet$ dimerization equals a potential shift of about −1.19 V for each redox step, which is larger than the difference between the oxidation potential of PhS$^-$ and **1**$^{2-}$. Thus, the S−S bond dissociation energy in **1** is smaller than in Ph_2S_2. This could be rationalized by the torsion angle of only 56° for the C−S−S−C unit in **1** due to the linked bipyridine units. This torsion angle deviates largely from the ideal value of 90° as in Ph_2S_2;[73] that is, the S−S bond in $^{S-S}$bpy is destabilized, which leads to a larger free energy for hydride transfer.

Table 2. Free Energy Contributions (kcal mol^{-1}) for the Hydricity and the BDFE$_{SH}$ of 1H$^-$ and PhS$^-$/PhSH[a]

	1H$^-$ (MeCN)	PhS$^-$/PhSH (dmso)
$\Delta G^\circ_{1,ox}$ (E_1)	−26.7 (−1.16)	−8.3 (−0.36)
$\Delta G^\circ_{2,ox}$ (E_2)	−26.7 (−1.16)	
$\Delta G^\circ_{3,H^+}$ (pK_a)	33.7 (24.7)	14.0 (10.3)
$\Delta G^\circ_{(H^+|H^-)}$	79.6	71.4
C_G	52.6	71.1
$\Delta G^\circ_{hydricity}$	60	14
ΔG°_{BDFE}(S−H)	59	76.9

[a]The redox potentials (V vs Fc$^{+|0}$) and the pK_a are given in parentheses.

The bond dissociation free energy (BDFE) for H atom abstraction is calculated according to eq 2 by using the recently revised C_G value of 52.6 kcal mol^{-1} in MeCN.[74]

$$\Delta G^\circ = 1.364\mathrm{p}K_a + 23.06E^\circ_1 + C_G \quad (2)$$

The BDFE of the S−H bond in **1**H$^-$ is 59 kcal mol^{-1}. Hence, the thermodynamic driving forces for H atom and H$^-$ transfer are almost the same, as initial reduction of **1** and of H$^\bullet$ to H$^-$ exhibit coincidently a similar potential in MeCN.[8] The BDFE for the H atom abstraction is considerably lower than for PhSH forming PhS$^\bullet$ in dmso (cf. BDFE^{PhSH} = 76.9 kcal mol^{-1}).[2] These BDFE values have been determined in different solvent media; however, it has been shown that the solvent has only a rather minor influence on the BDFE as no charged species are formed.[74] Having again a closer look on the individual free energy contributions, we can conclude that the slightly higher pK_a of **1**H$^-$ in comparison to PhSH would actually lead to a slightly larger BDFE in **1**H$^-$ than in PhSH; however, this effect is overbalanced by the stabilization of the radical by the adjacent thiolate function, giving a single-electron S−S bond (2-center−3-electron) in **1**$^-$.[75] Indeed, the difference in the S−S bond dissociation free energy of the radical $Ph_2S_2^-$ and Ph_2S_2 in dmf has been estimated to be 33 kcal mol^{-1},[75] which in turn gives a BDFE of about 22 kcal mol^{-1} for $Ph_2S_2^-$ (cf. BDE(Ph_2S_2) = 55 kcal mol^{-1}).

PCET Reactivity. At first, we explored the electrochemical PCET reactivity by CV. Adding TFE or [HNEt$_3$]PF$_6$ indeed affects the redox behavior of **1**. TFE has an effective pK_a of about 25.9[76] in MeCN considering homoconjugation, which is slightly higher than the one of **1**$^{2-}$, whereas the pK_a of [HNEt$_3$]PF$_6$ with 18.83[56] is lower. The initial cathodic feature is virtually not affected by the acids, indicating that **1** and **1**$^-$ are not protonated by the acids and thus have a lower pK_a than that of [HNEt$_3$]PF$_6$ (Figure 5). This also implies that the shift of the potential upon protonation is rather large, which is in agreement with a previous report on a pK_a of 8.4 for the radical anion of 3,8-diiodo-1,2-dithiino[4,3-*b*:5,6-*b*′]dipyridine in CH_2Cl_2.[77] The anodic features in the CV data are shifted to less negative potentials with increasing acid strengths, which is in line with expectations: **1**H$^-$, which is in equilibrium with **1**$^{2-}$, should be harder to oxidize than **1**$^{2-}$ due to the charge compensation upon protonation. The CV data of **1** and TFE show two further irreversible cathodic processes, a shoulder at a potential of ∼−2.1 V, and third reduction at a peak potential

https://doi.org/10.1021/jacs.1c01763
J. Am. Chem. Soc. 2021, 143, 6238−6247

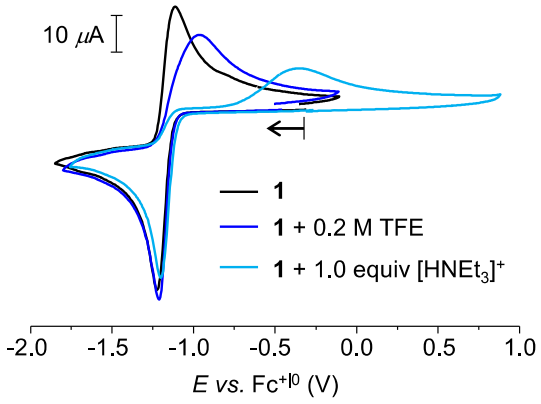

Figure 5. CV data of **1** without and with an acid, TFE or $[HNEt_3]PF_6$, in MeCN, $[^nBu_4N]PF_6$, ν = 0.1 V s^{-1}, rt.

of −2.26 V, which is about 0.4 V less negative than in the absence of protons due to the charge compensation by protonation (ν = 0.1 V s^{-1}, Figure S3, blue trace).

Subsequently, we probed the $1H^+/2e^-$ reactivity of $1H^-$ with two different hydride acceptors. The reaction of *in situ* generated $1H^-$ with 1.0 equiv of the acridinium hydride acceptor Ph-Acr$^+$ at 25 °C in MeCN-d_3 afforded **1** concomitant with the formation of Ph-AcrH[78] (Figure 6 and

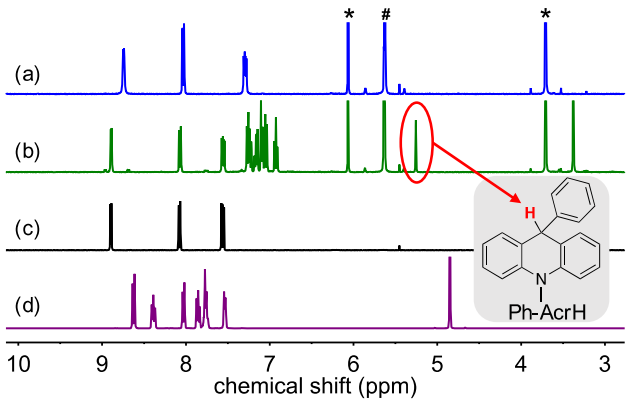

Figure 6. ^{1}H NMR spectra (400 MHz, MeCN-d_3 at 243 K) of (a) $1H^-$, (b) the reaction of $1H^-$ with $[Ph\text{-}Acr]ClO_4$ proceeding at 25 °C, (c) **1**, and (d) $[Ph\text{-}Acr]ClO_4$. ∗: 1,3,5-trimethoxybenzene; #: $[CoCp_2]^+$.

Figure S28; $[Ph\text{-}Acr]ClO_4$ = 10-methyl-9-phenylacridinium perchlorate, $\Delta G^\circ_{H^-}$ = 76 kcal mol^{-1} in MeCN).[15] Monitoring of the reaction progress by ^{1}H NMR spectroscopy using the internal standard 1,3,5-trimethoxybenzene showed that the reaction was almost completed after 3 h at 25 °C and proceeds with 90% spectroscopic yield (Figure S22). On the other hand, when $1H^-$ was mixed with 5.0 equiv of BIM$^+$, no hydride transfer reactivity was observed after monitoring the reaction at rt for more than 30 h; $1H^-$ just slowly converts to **2** (Figure S23; $[BIM]PF_6$ = 1,3-dimethyl-2-phenylbenzimidazolium hexafluorophosphate, $\Delta G^\circ_{H^-}$ = 50 kcal mol^{-1} in MeCN).[15] This reactivity is in line with the hydricity determined by the potential−pK_a method as BIMH is a stronger hydride donor then $1H^-$.

Finally, the $1H^+/1e^-$ reactivity of $1H^-$, i.e., hydrogen atom transfer, has been examined by reacting $1H^-$ with the hydrogen atom acceptors TEMPO$^\bullet$ and 2,4,6-TTBP$^\bullet$ in MeCN-d_3, both of which have stronger X−H bonds than $1H^-$ (TEMPO$^\bullet$ = 2,2,6,6-tetramethylpiperidine-*N*-hydroxy radical, BDFE = 64 kcal mol^{-1};[2] 2,4,6-TTBP$^\bullet$ = 2,4,6-tri-*tert*-butylphenoxy radical, BDFE = 75 kcal mol^{-1}).[79] $1H^-$ was again prepared *in situ* at −30 °C, and 1.0 equiv 1,3,5-trimethoxybenzene was added as internal standard. The reaction of $1H^-$ with 1.0 equiv of TEMPO$^\bullet$ was completed after around 30 min at 25 °C. The resulting ^{1}H NMR spectrum features the characteristic resonances of TEMPO-H and **2**, respectively, evidencing that the net HAT reaction has occurred (Figures S24 and S29). The formation of **2** indicates that 1^- is not stable and undergoes sulfur extrusion at 25 °C. When the reaction was pursued at −30 °C, quantitative formation of TEMPO-H was observed after 5 h (Figures S25 and S30), together with a new set of ^{1}H NMR resonances located in between those of **1** and 1^{2-}, which can be rationalized by redox equilibria of **1**, 1^-, and 1^{2-}. In fact, 1^- has the same potential for the oxidation and reduction, leading to a disproportionation equilibrium K_{dis} according to eq 3, where n is the number of transferred electrons, F is Faraday's constant, R is the gas constant, T is the temperature, and ΔE is the difference in redox potentials:

$$K_{dis} = \exp\left(\frac{nF}{RT}\Delta E\right) \quad (3)$$

Thus, the averaged proton resonances may originate from fast electron exchange between **1**, 1^-, and 1^{2-} on the NMR time scale. Indeed, a 1:1 mixture of **1** and *in situ* prepared 1^{2-} leads to an averaged set of ^{1}H NMR signals akin to the ones observed after the HAT reaction (Figure S26). The stoichiometric reaction of *in situ* prepared $1H^-$ with the stronger H atom acceptor 2,4,6-TTBP$^\bullet$ proceeds faster. After 7 min full conversion was observed at −30 °C by ^{1}H NMR spectroscopy alongside the averaged signal set for **1**, 1^-, and 1^{2-} (Figures S27 and S31).

These reactions show that $1H^-$ indeed undergoes facile hydride and H atom transfer and that the free energy values for $H^-/H^\bullet$ transfer as determined via the reduction potentials and the pK_a of the species involved are in line with the observed reactivity.

CONCLUSION

We have comprehensively established the thermodynamics of a bioinspired PCET reagent $1H^-$ having a unique preorganized S−H···$^-$S unit in the backbone of a metal-bound bipyridine ligand, which is capable of serving as a proton, H atom, or hydride donor. The study demonstrates that the design principle of biological hydride transfer reagents, e.g., flavins, can be transferred to synthetic reagents. Because of its distinct geometric and electronic properties, $1H^-$ is a smooth PCET reagent featuring moderate hydricity and a relatively low BDFE ($\Delta G^\circ_{H^-}$ = 60 kcal mol^{-1}, $\Delta G^\circ_{H^\bullet}$ = 59 kcal mol^{-1}). Metal binding of the bipyridine unit constrains the structural flexibility of the ligand, which largely impacts the redox chemistry of the peripheral disulfide/dithiol switch: (i) the disulfide species is destabilized due to the nonideal C−S−S−C torsion angle of only 56°, (ii) the radical intermediate is stabilized due to the adjacent thiolate function, and (iii) the low reorganization energies due to geometric constraints facilitate two electrochemically reversible 1e$^-$ reduction processes. Thus, the formation of $1H^-$ can be accomplished under mild conditions, that is, at a moderately negative potential of −1.16 V with weak acids, which makes it a

https://doi.org/10.1021/jacs.1c01763
J. Am. Chem. Soc. 2021, 143, 6238−6247

promising reagent for electrochemically driven PCET transformations of substrates. Furthermore, $\mathbf{1}H^-$ overcomes the drawback of many metal-free hydride donors, which show a large gap between the first and second reduction process[15] and detrimental side reactions of the radical intermediate. Future studies in our laboratories will focus on the kinetic hydricity and the transfer mechanism of $\mathbf{1}H^-$, e.g., stepwise vs concerted, to exploit its use as a hydride transfer reagent under mild conditions. In addition, the modified bipyridine ligand may be attached to a wide variety of metal complex fragments of different basicity and size, and it is an interesting perspective that this may be used for tuning the thermodynamics of PCET reactivity at the peripheral S−H···$^-$S site.

■ ASSOCIATED CONTENT

Supporting Information

The Supporting Information is available free of charge at https://pubs.acs.org/doi/10.1021/jacs.1c01763.

Synthesis and characterizations of **1**, $\mathbf{1}^{2-}$, $\mathbf{1}H^-$, and **2**, electrochemical data, thermodynamic considerations, examination of CO_2 reduction, UV−vis titration experiments, ^{1}H NMR experiments of hydride transfer and HAT reactivity, ESI-MS, IR and NMR spectra, details of DFT calculations, and Cartesian coordinates (PDF)

Accession Codes

CCDC 2061946−2061947 contain the supplementary crystallographic data for this paper. These data can be obtained free of charge via www.ccdc.cam.ac.uk/data_request/cif, or by emailing data_request@ccdc.cam.ac.uk, or by contacting The Cambridge Crystallographic Data Centre, 12 Union Road, Cambridge CB2 1EZ, UK; fax: +44 1223 336033.

■ AUTHOR INFORMATION

Corresponding Authors

Franc Meyer − *Universität Göttingen, Institut für Anorganische Chemie and International Center for Advanced Studies of Energy Conversion (ICASEC), D-37077 Göttingen, Germany;* orcid.org/0000-0002-8613-7862; Email: franc.meyer@chemie.uni-goettingen.de

Inke Siewert − *Universität Göttingen, Institut für Anorganische Chemie and International Center for Advanced Studies of Energy Conversion (ICASEC), D-37077 Göttingen, Germany;* orcid.org/0000-0003-3121-3917; Email: inke.siewert@chemie.uni-goettingen.de

Authors

Shao-An Hua − *Universität Göttingen, Institut für Anorganische Chemie, D-37077 Göttingen, Germany*

Lucas A. Paul − *Universität Göttingen, Institut für Anorganische Chemie, D-37077 Göttingen, Germany*

Manuel Oelschlegel − *Universität Göttingen, Institut für Anorganische Chemie, D-37077 Göttingen, Germany*

Sebastian Dechert − *Universität Göttingen, Institut für Anorganische Chemie, D-37077 Göttingen, Germany;* orcid.org/0000-0002-2864-2449

Complete contact information is available at: https://pubs.acs.org/10.1021/jacs.1c01763

Funding

This work was supported by funding from the Deutsche Forschungsgemeinschaft (DFG, German Research Foundation) via projects Me1313/15-1 within the SPP 2102 (F.M.), SI 1577/2 (I.S.), and SFB 1073 C01 (I.S.) and by the Georg-August-Universität Göttingen.

Notes

The authors declare no competing financial interest.

■ ACKNOWLEDGMENTS

This paper is dedicated to Prof. Dr. Kaim on the occasion of his 70th birthday.

■ REFERENCES

(1) Costentin, C.; Robert, M.; Saveant, J. M. Update 1 of: Electrochemical Approach to the Mechanistic Study of Proton-Coupled Electron Transfer. *Chem. Rev.* **2010**, *110*, PR1−40.

(2) Warren, J. J.; Tronic, T. A.; Mayer, J. M. Thermochemistry of Proton-Coupled Electron Transfer Reagents and its Implications. *Chem. Rev.* **2010**, *110*, 6961−7001.

(3) Waidmann, C. R.; Miller, A. J.; Ng, C.-W. A.; Scheuermann, M. L.; Porter, T. R.; Tronic, T. A.; Mayer, J. M. Using Combinations of Oxidants and Bases as PCET Reactants: Thermochemical and Practical Considerations. *Energy Environ. Sci.* **2012**, *5*, 7771−7780.

(4) Weinberg, D. R.; Gagliardi, C. J.; Hull, J. F.; Murphy, C. F.; Kent, C. A.; Westlake, B. C.; Paul, A.; Ess, D. H.; McCafferty, D. G.; Meyer, T. J. Proton-Coupled Electron Transfer. *Chem. Rev.* **2012**, *112*, 4016−4093.

(5) Hu, Y.; Shaw, A. P.; Estes, D. P.; Norton, J. R. Transition-Metal Hydride Radical Cations. *Chem. Rev.* **2016**, *116*, 8427−8462.

(6) Maity, A.; Teets, T. S. Main Group Lewis Acid-Mediated Transformations of Transition-Metal Hydride Complexes. *Chem. Rev.* **2016**, *116*, 8873−8911.

(7) Morris, R. H. Bronsted-Lowry Acid Strength of Metal Hydride and Dihydrogen Complexes. *Chem. Rev.* **2016**, *116*, 8588−8654.

(8) Wiedner, E. S.; Chambers, M. B.; Pitman, C. L.; Bullock, R. M.; Miller, A. J.; Appel, A. M. Thermodynamic Hydricity of Transition Metal Hydrides. *Chem. Rev.* **2016**, *116*, 8655−8692.

(9) Darcy, J. W.; Koronkiewicz, B.; Parada, G. A.; Mayer, J. M. A Continuum of Proton-Coupled Electron Transfer Reactivity. *Acc. Chem. Res.* **2018**, *51*, 2391−2399.

(10) Hammes-Schiffer, S. Controlling Electrons and Protons through Theory: Molecular Electrocatalysts to Nanoparticles. *Acc. Chem. Res.* **2018**, *51*, 1975−1983.

(11) Ilic, S.; Pandey Kadel, U.; Basdogan, Y.; Keith, J. A.; Glusac, K. D. Thermodynamic Hydricities of Biomimetic Organic Hydride Donors. *J. Am. Chem. Soc.* **2018**, *140*, 4569−4579.

(12) Milan, M.; Salamone, M.; Costas, M.; Bietti, M. The Quest for Selectivity in Hydrogen Atom Transfer Based Aliphatic C−H Bond Oxygenation. *Acc. Chem. Res.* **2018**, *51*, 1984−1995.

(13) Ghosh, D.; Kumar, G. R.; Subramanian, S.; Tanaka, K. More Than Just a Reagent: The Rise of Renewable Organohydrides for Catalytic Reduction of Carbon Dioxide. *ChemSusChem* **2021**, *14*, 824−841.

(14) Luo, J.; Rauch, M.; Avram, L.; Ben-David, Y.; Milstein, D. Catalytic Hydrogenation of Thioesters, Thiocarbamates, and Thioamides. *J. Am. Chem. Soc.* **2020**, *142*, 21628−21633.

(15) Ilic, S.; Alherz, A.; Musgrave, C. B.; Glusac, K. D. Thermodynamic and Kinetic Hydricities of Metal-Free Hydrides. *Chem. Soc. Rev.* **2018**, *47*, 2809−2836.

(16) Deponte, M. Glutathione Catalysis and the Reaction Mechanisms of Glutathione-Dependent Enzymes. *Biochim. Biophys. Acta, Gen. Subj.* **2013**, *1830*, 3217−3266.

(17) Meister, A. Glutathione Metabolism and its Selective Modification. *J. Biol. Chem.* **1988**, *263*, 17205−17208.

(18) Mannervik, B. The Enzymes of Glutathione Metabolism: An Overview. *Biochem. Soc. Trans.* **1987**, *15*, 717−718.

(19) Sousa, S. F.; Neves, R. P. P.; Waheed, S. O.; Fernandes, P. A.; Ramos, M. J. Structural and Mechanistic Aspects of S-S Bonds in the Thioredoxin-Like Family of Proteins. *Biol. Chem.* **2019**, *400*, 575−587.

(20) Wang, J.; Zhou, Y.-G. Organocatalytic Transfer Hydrogenation. In *Homogeneous Hydrogenation with Non-Precious Catalysts*; Teichert, J. F., Ed.; Wiley: 2019; pp 261−284.
(21) Wang, J.; Zhao, Z.-B.; Zhao, Y.; Luo, G.; Zhu, Z.-H.; Luo, Y.; Zhou, Y.-G. Chiral and Regenerable NAD(P)H Models Enabled Biomimetic Asymmetric Reduction: Design, Synthesis, Scope, and Mechanistic Studies. *J. Org. Chem.* **2020**, *85*, 2355−2368.
(22) Kim, A. N.; Stoltz, B. M. Recent Advances in Homogeneous Catalysts for the Asymmetric Hydrogenation of Heteroarenes. *ACS Catal.* **2020**, *10*, 13834−13851.
(23) Chen, Q.-A.; Gao, K.; Duan, Y.; Ye, Z.-S.; Shi, L.; Yang, Y.; Zhou, Y.-G. Dihydrophenanthridine: A New and Easily Regenerable NAD(P)H Model for Biomimetic Asymmetric Hydrogenation. *J. Am. Chem. Soc.* **2012**, *134*, 2442−2448.
(24) Zheng, C.; You, S.-L. Transfer Hydrogenation with Hantzsch Esters and Related Organic Hydride Donors. *Chem. Soc. Rev.* **2012**, *41*, 2498−2518.
(25) Wang, P.-Z.; Chen, J.-R.; Xiao, W.-J. Hantzsch Esters: An Emerging Versatile Class of Reagents in Photoredox Catalyzed Organic Synthesis. *Org. Biomol. Chem.* **2019**, *17*, 6936−6951.
(26) Ouellet, S. G.; Walji, A. M.; MacMillan, D. W. Enantioselective Organocatalytic Transfer Hydrogenation Reactions Using Hantzsch Esters. *Acc. Chem. Res.* **2007**, *40*, 1327−1339.
(27) You, S.-L. Recent Developments in Asymmetric Transfer Hydrogenation with Hantzsch Esters: A Biomimetic Approach. *Chem. - Asian J.* **2007**, *2*, 820−827.
(28) McSkimming, A.; Colbran, S. B. The Coordination Chemistry of Organo-Hydride Donors: New Prospects for Efficient Multi-Electron Reduction. *Chem. Soc. Rev.* **2013**, *42*, 5439−5488.
(29) Ghosh, D.; Kobayashi, K.; Kajiwara, T.; Kitagawa, S.; Tanaka, K. Catalytic Hydride Transfer to CO_2 Using Ru-NAD-Type Complexes under Electrochemical Conditions. *Inorg. Chem.* **2017**, *56*, 11066−11073.
(30) Koizumi, T. A.; Tanaka, K. Reversible hydride generation and release from the ligand of $[Ru(pbn)(bpy)_2](PF_6)_2$ driven by a pbn-localized redox reaction. *Angew. Chem., Int. Ed.* **2005**, *44*, 5891−5894.
(31) Tannai, H.; Koizumi, T. A.; Wada, T.; Tanaka, K. Electrochemical and Photochemical Behavior of a Ruthenium(II) complex Bearing Two Redox Sites as a Model for the NAD^+/NADH Redox Couple. *Angew. Chem., Int. Ed.* **2007**, *46*, 7112−7115.
(32) Polyansky, D.; Cabelli, D.; Muckerman, J. T.; Fujita, E.; Koizumi, T. A.; Fukushima, T.; Wada, T.; Tanaka, K. Photochemical and Radiolytic Production of an Organic Hydride Donor with a Ru(II) Complex Containing an NAD^+ Model Ligand. *Angew. Chem., Int. Ed.* **2007**, *46*, 4169−4172.
(33) McLoughlin, E. A.; Waldie, K. M.; Ramakrishnan, S.; Waymouth, R. M. Protonation of a Cobalt Phenylazopyridine Complex at the Ligand Yields a Proton, Hydride, and Hydrogen Atom Transfer Reagent. *J. Am. Chem. Soc.* **2018**, *140*, 13233−13241.
(34) Charette, B. J.; Ziller, J. W.; Heyduk, A. F. Metal-Ion Influence on Ligand-Centered Hydrogen-Atom Transfer. *Inorg. Chem.* **2021**, *60*, 1579−1589.
(35) Charette, B. J.; Ziller, J. W.; Heyduk, A. F. Exploring Ligand-Centered Hydride and H-Atom Transfer. *Inorg. Chem.* **2021**, *60*, 5367−5375.
(36) Giles, N. M.; Giles, G. I.; Jacob, C. Multiple Roles of Cysteine in Biocatalysis. *Biochem. Biophys. Res. Commun.* **2003**, *300*, 1−4.
(37) Giles, N. M.; Watts, A. B.; Giles, G. I.; Fry, F. H.; Littlechild, J. A.; Jacob, C. Metal and Redox Modulation of Cysteine Protein Function. *Chem. Biol.* **2003**, *10*, 677−693.
(38) Paulsen, C. E.; Carroll, K. S. Cysteine-Mediated Redox Signaling: Chemistry, Biology, and Tools for Discovery. *Chem. Rev.* **2013**, *113*, 4633−4679.
(39) Cattaneo, M.; Schiewer, C. E.; Schober, A.; Dechert, S.; Siewert, I.; Meyer, F. 2,2′-Bipyridine Equipped with a Disulfide/Dithiol Switch for Coupled Two-Electron and Two-Proton Transfer. *Chem. - Eur. J.* **2018**, *24*, 4864−4870.
(40) Hua, S.-A.; Cattaneo, M.; Oelschlegel, M.; Heindl, M.; Schmid, L.; Dechert, S.; Wenger, O. S.; Siewert, I.; Gonzalez, L.; Meyer, F. Electrochemical and Photophysical Properties of Ruthenium(II) Complexes Equipped with Sulfurated Bipyridine Ligands. *Inorg. Chem.* **2020**, *59*, 4972−4984.
(41) Heindl, M.; Hongyan, J.; Hua, S.-A.; Oelschlegel, M.; Meyer, F.; Schwarzer, D.; Gonzalez, L. Excited-State Dynamics of $[Ru(^{S-S}bpy)(bpy)_2]^{2+}$ to Form Long-Lived Localized Triplet States. *Inorg. Chem.* **2021**, *60*, 1672−1682.
(42) Thomas, A. M.; Lin, B.-L.; Wasinger, E. C.; Stack, T. D. Ligand Noninnocence of Thiolate/Disulfide in Dinuclear Copper Complexes: Solvent-Dependent Redox Isomerization and Proton-Coupled Electron Transfer. *J. Am. Chem. Soc.* **2013**, *135*, 18912−18919.
(43) Ording-Wenker, E. C.; van der Plas, M.; Siegler, M. A.; Fonseca Guerra, C.; Bouwman, E. Protonation of a Biologically Relevant Cu(II) μ-thiolate Complex: Ligand Dissociation or Formation of a Protonated Cu(I) Disulfide Species? *Chem. - Eur. J.* **2014**, *20*, 16913−16921.
(44) Cattaneo, M.; Guo, F.; Kelly, H. R.; Videla, P. E.; Kiefer, L.; Gebre, S.; Ge, A.; Liu, Q.; Wu, S.; Lian, T.; Batista, V. S. Robust Binding of Disulfide-Substituted Rhenium Bipyridyl Complexes for CO_2 Reduction on Gold Electrodes. *Front. Chem.* **2020**, *8*, 86.
(45) Ching, H. Y. V.; Wang, X.; He, M.; Perujo Holland, N.; Guillot, R.; Slim, C.; Griveau, S.; Bertrand, H. C.; Policar, C.; Bedioui, F.; Fontecave, M. Rhenium Complexes Based on 2-Pyridyl-1,2,3-triazole Ligands: A New Class of CO_2 Reduction Catalysts. *Inorg. Chem.* **2017**, *56*, 2966−2976.
(46) Kurz, P.; Probst, B.; Spingler, B.; Alberto, R. Ligand Variations in $[ReX(diimine)(CO)_3]$ Complexes: Effects on Photocatalytic CO_2 Reduction. *Eur. J. Inorg. Chem.* **2006**, 2966−2974.
(47) Boyd, R. J.; Perkyns, J. S.; Ramani, R. Conformations of Simple Disulfides and L-Cystine. *Can. J. Chem.* **1983**, *61*, 1082−1085.
(48) Vogler, A.; Shenderovich, I. G. Photochemistry of Deprotonated Rhenium(I) (3,3′-dihydroxy-2,2′-bipyridine) Tricarbonyl Chloride. Photoisomerization at the Chelate in Basic Solution. *Inorg. Chim. Acta* **2014**, *421*, 496−499.
(49) Paul, L. A.; Röttcher, N. C.; Zimara, J.; Borter, J.-H.; Du, J.-P.; Schwarzer, D.; Mata, R. A.; Siewert, I. Photochemical Properties of $Re(CO)_3$ Complexes with and without a Local Proton Source and Implications for CO_2 Reduction Catalysis. *Organometallics* **2020**, *39*, 2405−2414.
(50) Hayashi, Y.; Kita, S.; Brunschwig, B. S.; Fujita, E. Involvement of a Binuclear Species with the Re−C(O)O−Re Moiety in CO_2 Reduction Catalyzed by Tricarbonyl Rhenium(I) Complexes with Diimine Ligands: Strikingly Slow Formation of the Re−Re and Re−C(O)O−Re Species From $Re(dmb)(CO)_3S$ (dmb = 4,4′-dimethyl-2,2′-bipyridine, S = solvent). *J. Am. Chem. Soc.* **2003**, *125*, 11976−11987.
(51) Worl, L. A.; Duesing, R.; Chen, P.; Ciana, L. D.; Meyer, T. J. Photophysical Properties of Polypyridyl Carbonyl Complexes of Rhenium (I). *J. Chem. Soc., Dalton Trans.* **1991**, 849−858.
(52) Fujita, E.; Muckerman, J. T. Why is Re−Re Bond Formation/Cleavage in $[Re(bpy)(CO)_3]_2$ Different from that in $[Re(CO)_5]_2$? Experimental and Theoretical Studies on the Dimers and Fragments. *Inorg. Chem.* **2004**, *43*, 7636−7647.
(53) Manbeck, G. F.; Muckerman, J. T.; Szalda, D. J.; Himeda, Y.; Fujita, E. Push or Pull? Proton Responsive Ligand Effects in Rhenium Tricarbonyl CO_2 Reduction Catalysts. *J. Phys. Chem. B* **2015**, *119*, 7457−7466.
(54) Kunkely, H.; Vogler, A. Optical Properties of (3,3′-dihydroxy-2,2′-bipyridine) Tricarbonyl-Rhenium(I) Chloride. Absorption and Emission Spectra. *Inorg. Chim. Acta* **2003**, *343*, 357−360.
(55) Connelly, N. G.; Geiger, W. E. Chemical Redox Agents for Organometallic Chemistry. *Chem. Rev.* **1996**, *96*, 877−910.
(56) McCarthy, B. D.; Martin, D. J.; Rountree, E. S.; Ullman, A. C.; Dempsey, J. L. Electrochemical Reduction of Brønsted Acids by Glassy Carbon in Acetonitrile-Implications for Electrocatalytic Hydrogen Evolution. *Inorg. Chem.* **2014**, *53*, 8350−8361.
(57) Tshepelevitsh, S.; Kütt, A.; Lõkov, M.; Kaljurand, I.; Saame, J.; Heering, A.; Plieger, P. G.; Vianello, R.; Leito, I. On the Basicity of

https://doi.org/10.1021/jacs.1c01763
J. Am. Chem. Soc. 2021, 143, 6238−6247

Organic Bases in Different Media. *Eur. J. Org. Chem.* **2019**, *2019*, 6735−6748.
(58) Leito, I.; Kaljurand, I.; Koppel, I. A.; Yagupolskii, L. M.; Vlasov, V. M. Spectrophotometric Acidity Scale of Strong Neutral Brønsted Acids in Acetonitrile. *J. Org. Chem.* **1998**, *63*, 7868−7874.
(59) Bordwell, F.; Cheng, J. P.; Harrelson, J. A. Homolytic Bond Dissociation Energies in Solution from Equilibrium Acidity and Electrochemical Data. *J. Am. Chem. Soc.* **1988**, *110*, 1229−1231.
(60) Tilset, M.; Parker, V. D. Solution Homolytic Bond Dissociation Energies of Organotransition-Metal Hydrides. *J. Am. Chem. Soc.* **1989**, *111*, 6711−6717.
(61) Berning, D. E.; Noll, B. C.; DuBois, D. L. Relative Hydride, Proton, and Hydrogen Atom Transfer Abilities of [HM-(diphosphine)$_2$]PF$_6$ Complexes (M = Pt, Ni). *J. Am. Chem. Soc.* **1999**, *121*, 11432−11447.
(62) DuBois, D. L.; Berning, D. E. Hydricity of Transition-Metal Hydrides and its Role in CO_2 Reduction. *Appl. Organomet. Chem.* **2000**, *14*, 860−862.
(63) Bausch, M.; Guadalupe-Fasano, C.; Gostowski, R. Estimates of Solution-Phase Bond Dissociation Energies for Carbon-Sulfur and Sulfur-Sulfur Bonds in Radical Anions Derived from Aromatic Sulfides. *Energy Fuels* **1991**, *5*, 419−423.
(64) Brereton, K. R.; Jadrich, C. N.; Stratakes, B. M.; Miller, A. J. M. Thermodynamic Hydricity Across Solvents: Subtle Electronic Effects and Striking Ligation Effects in Iridium Hydrides. *Organometallics* **2019**, *38*, 3104−3110.
(65) Burgess, S. A.; Appel, A. M.; Linehan, J. C.; Wiedner, E. S. Changing the Mechanism for CO_2 Hydrogenation Using Solvent-Dependent Thermodynamics. *Angew. Chem., Int. Ed.* **2017**, *56*, 15002−15005.
(66) Ceballos, B. M.; Tsay, C.; Yang, J. Y. CO_2 Reduction or HCO_2^- oxidation? Solvent-Dependent Thermochemistry of a Nickel Hydride Complex. *Chem. Commun.* **2017**, *53*, 7405−7408.
(67) Connelly, S. J.; Wiedner, E. S.; Appel, A. M. Predicting the Reactivity of Hydride Donors in Water: Thermodynamic Constants for Hydrogen. *Dalton Trans.* **2015**, *44*, 5933−5938.
(68) Tsay, C.; Livesay, B. N.; Ruelas, S.; Yang, J. Y. Solvation Effects on Transition Metal Hydricity. *J. Am. Chem. Soc.* **2015**, *137*, 14114−14121.
(69) Himmel, D.; Goll, S. K.; Leito, I.; Krossing, I. A Unified pH Scale for All Phases. *Angew. Chem., Int. Ed.* **2010**, *49*, 6885−6888.
(70) Radtke, V.; Himmel, D.; Putz, K.; Goll, S. K.; Krossing, I. The Protoelectric Potential Map (PPM): An Absolute Two-Dimensional Chemical Potential Scale for a Global Understanding of Chemistry. *Chem. - Eur. J.* **2014**, *20*, 4194−4211.
(71) A similar value of 20.9 in MeCN is obtained when the empirical formula of Leito and co-workers was used to convert the acidity between MeCN and dmso, which was derived from experimental values in dmso and MeCN. Kütt, A.; Selberg, S.; Kaljurand, I.; Tshepelevitsh, S.; Heering, A.; Darnell, A.; Kaupmees, K.; Piirsalu, M.; Leito, I. pK_a Values in Organic Chemistry - Making Maximum Use of the Available Data. *Tetrahedron Lett.* **2018**, *59*, 3738−3748.
(72) Nam, P. C.; Nguyen, M. T.; Chandra, A. K. Theoretical Study of the Substituent Effects on the S−H bond Dissociation Energy and Ionization Energy of 3-pyridinethiol: Prediction of Novel Antioxidant. *J. Phys. Chem. A* **2006**, *110*, 10904−10911.
(73) Raisanen, M. T.; Runeberg, N.; Klinga, M.; Nieger, M.; Bolte, M.; Pyykko, P.; Leskela, M.; Repo, T. Coordination of Pyridinethiols in Gold(I) Complexes. *Inorg. Chem.* **2007**, *46*, 9954−9960.
(74) Wise, C. F.; Agarwal, R. G.; Mayer, J. M. Determining Proton-Coupled Standard Potentials and X−H Bond Dissociation Free Energies in Nonaqueous Solvents Using Open-Circuit Potential Measurements. *J. Am. Chem. Soc.* **2020**, *142*, 10681−10691.
(75) Antonello, S.; Daasbjerg, K.; Jensen, H.; Taddei, F.; Maran, F. Formation and Cleavage of Aromatic Disulfide Radical Anions. *J. Am. Chem. Soc.* **2003**, *125*, 14905−14916.
(76) Lam, Y. C.; Nielsen, R. J.; Gray, H. B.; Goddard, W. A. A Mn Bipyrimidine Catalyst Predicted To Reduce CO_2 at Lower Overpotential. *ACS Catal.* **2015**, *5*, 2521−2528.
(77) Benniston, A. C.; Allen, B. D.; Harriman, A.; Llarena, I.; Rostron, J. P.; Stewart, B. Accessing Molecular Memory via a Disulfide Switch. *New J. Chem.* **2009**, *33*, 417−427.
(78) Yang, X.; Walpita, J.; Zhou, D.; Luk, H. L.; Vyas, S.; Khnayzer, R. S.; Tiwari, S. C.; Diri, K.; Hadad, C. M.; Castellano, F. N.; Krylov, A. I.; Glusac, K. D. Toward Organic Photohydrides: Excited-State Behavior of 10-Methyl-9-phenyl-9,10-dihydroacridine. *J. Phys. Chem. B* **2013**, *117*, 15290−15296.
(79) Recalculated from the values given in ref 2 with the revised C_G value from ref 74.

https://doi.org/10.1021/jacs.1c01763
J. Am. Chem. Soc. 2021, 143, 6238−6247